PHYSICAL REVIEW B **96**, 201102(R) (2017)

Ferromagnetic Weyl semimetal phase in a tetragonal structure

Y. J. Jin,[1] R. Wang,[1,2] Z. J. Chen,[1,3] J. Z. Zhao,[1,4] Y. J. Zhao,[3] and H. Xu[1,*]

[1]*Department of Physics, South University of Science and Technology of China, Shenzhen 518055, People's Republic of China*
[2]*Institute for Structure and Function & Department of Physics, Chongqing University, Chongqing 400044, People's Republic of China*
[3]*Department of Physics, South China University of Technology, Guangzhou 510640, People's Republic of China*
[4]*Dalian Institute of Chemical Physics, Chinese Academy of Sciences, Dalian 116023, People's Republic of China*

(Received 11 June 2017; revised manuscript received 31 August 2017; published 2 November 2017)

Magnetic topological semimetals have drawn significant interest since they can combine band topology with intrinsic magnetic order. Here, we propose that ideal Weyl semimetal features can coexist with a ferromagnetic (FM) ground state in a class of compounds with centrosymmetric tetragonal structures. In this magnetic system with inversion symmetry, the direction of magnetization is able to manipulate the symmetry protected band structures from a node-line type to a Weyl one in the presence of spin-orbital coupling. The FM node-line semimetal phase is protected by mirror symmetry with the reflection-invariant plane perpendicular to the magnetic order. Within mirror symmetry breaking due to magnetization along other directions, the gapless node-line loop will degenerate to only one pair of Weyl points protected by rotational symmetry along the magnetic axis, which is largely separated in momentum space. Such a FM Weyl semimetal phase offers a nice platform with a minimum number of Weyl points in a condensed matter system. These findings provide several realistic candidates for the investigation of topological semimetals with time-reversal symmetry breaking, especially demonstrating the use of system symmetry as a powerful recipe for discovering FM Weyl semimetals with attractive features.

DOI: 10.1103/PhysRevB.96.201102

Magnetic topological materials, including topological insulators (TIs) [1–5] and topological semimetals (TSMs) [6–8] in their quantum-well structures with time-reversal (TR) symmetry breaking, have attracted intensive attention recently. Distinguished from gapped magnetic TIs, magnetic TSMs host finite numbers or continuous nodal lines of band crossing points near the Fermi level in momentum space. Such crystal symmetry protected features lead to exotic conductive surface states, which are Fermi arcs in Weyl semimetals (WSMs) [7] and drumhead states in node-line semimetals (NLSMs) [9]. The realization of these robust spin-dependent surface states is a key step in achieving unusual spectroscopic and transport phenomena, especially the experimental observation of the quantum anomalous Hall effect (QAHE).

Up to now, nonmagnetic TSMs have been studied intensively [10–20], but only a few magnetic TSMs have been proposed [6,8,21,22]. For instance, magnetic $HgCr_2Se_4$, defined as a Chern semimetal, has been predicted to host two nodal points [6], which does not fully satisfy the WSM features since each crossing point possesses a chiral charge of 2. So far, the nontrivial properties of $HgCr_2Se_4$ have not been verified experimentally [23,24]. Antiferromagnetic (AFM) $YbMnBi_2$ [21] and Mn_3X (X = Ge, Sn) [22] were proposed to possess TR breaking Weyl fermions, and especially the latter exhibits a large anomalous Hall effect due to a noncollinear AFM configuration [25,26]. Very recently, magnetic Heusler alloys were also predicted to host the topology of WSMs [8,27]. However, the energies of the Weyl points are much higher (∼0.6 eV) above the Fermi level, therefore challenges remain on manipulating Weyl points relative to the Fermi level [8] for future applications. The identification of materials with easily observable ferromagnetic (FM) Weyl fermions thus defines an important problem in the study of this topological phase.

In this Rapid Communication, we will begin by recalling the topological constraints that spatial inversion symmetry imposes in magnetic materials, in which the spin degeneracy of electronic bands is removed by breaking TR symmetry. In a three-dimensional system with breaking TR but keeping spatial inversion, the topological behaviors are determined by the parity eigenvalues of occupied states at eight TR invariant momenta (TRIM) points $k_{\rm inv}$ [28,29]. If the product $\chi_P = \prod_{k_{\rm inv}; i\in {\rm occ}} \zeta_i(k_{\rm inv})$ of the inversion eigenvalues of occupied bands at all TRIM points is -1, this implies that the system may be a WSM, coexisting with an odd number of pairs of Weyl points [28]. This allows us to explore or design the topological electronic properties of WSMs based on the parities of occupied bands. We will then perform first-principles calculations and high-throughput screening of the band-structure topology of materials in the inorganic crystal structure database (ISCD) [30]. The existence of a FM WSM phase in the experimentally synthesized compounds β-V_2OPO_4 [31–33] and Co_2S_2Tl [34,35] is predicted. Using high-throughput calculations, we also predict a class of materials Fe_2S_2X (X = Al, Ga, In) that can possess the same topological features. All of the above compounds share a body-centered-tetragonal (bct) structure with inversion symmetry. Although these candidates have different chemical formulas and even space groups, our symmetry analysis shows that the symmetry protected band topology is due to their identical magnetic space group with a fixed magnetization axis. The topological phase, such as FM NLSM and WSM features, can be switched by changing magnetization directions. The NLSM band structure with spin-orbital coupling (SOC) is protected by mirror reflection symmetry with the reflection-invariant plane perpendicular to the spin-polarized direction. This gapless node-line loop will degenerate to one pair of well-separated Weyl points once mirror reflection symmetry is broken by varying the magnetization directions. In such a case, these systems possess the minimum number of Weyl points in a

*xuh@sustc.edu.cn

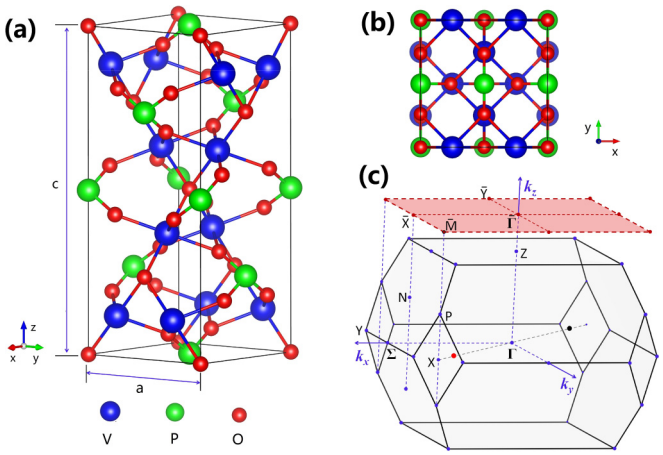

FIG. 1. Crystal structure and Brillouin zone (BZ). (a) Side and (b) top views of the crystal structure of β-V_2OPO_4 with space group $I4_1amd$ (No. 141). V, P, and O atoms are represented by blue, green, and red spheres, respectively. (c) The body-centered-tetragonal (bct) BZ and the corresponding (001) surface BZ. The high-symmetry points are indicated. Two Weyl points with opposite chirality are symmetrically located at the Γ-X axis as red ($C = +1$) and black ($C = -1$) dots, with magnetization along the [110] direction.

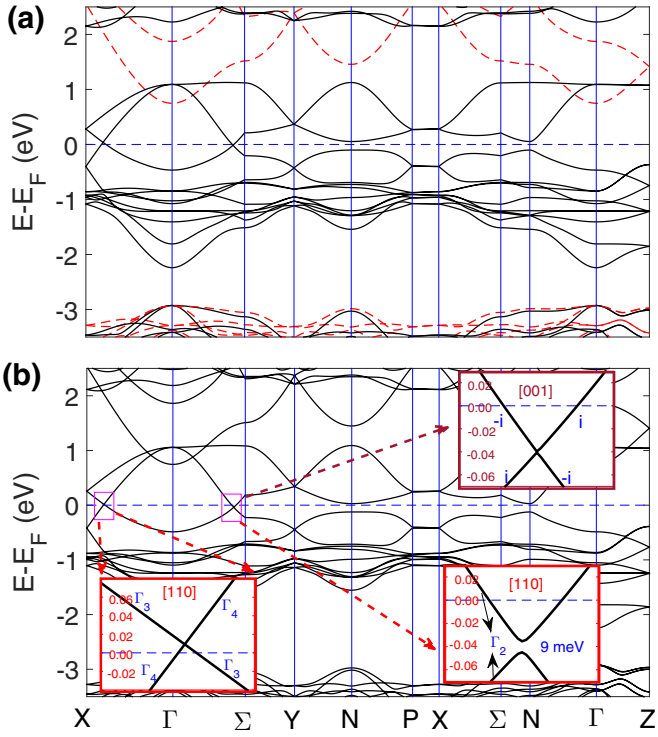

FIG. 2. (a) The band structure of β-V_2OPO_4 along high-symmetry lines without spin-orbital coupling (SOC). The majority and minority spin bands are denoted by the solid (black) and dashed (red) lines, respectively. (b) Band structure with SOC. The upper right inset represents the bands in the Γ-Σ direction with a [001] magnetization direction, and each band corresponds to either of the mirror eigenvalues i and $-i$. The lower left and right panels respectively denote the bands in the Γ-X and Γ-Σ directions with a [110] magnetization direction. The two crossing bands in Γ-X respectively belong to the two irreducible representations Γ_3 and Γ_4 of C_2^{110}.

condensed matter system. In the main text, we will use the vanadium phosphorus oxide β-V_2OPO_4, a realistic material synthesized in 1989 [33], as an example to illustrate the topologically nontrivial features of this class of materials with tetragonal symmetry. Detailed results of the other compounds are given in the Supplemental Material (SM) [36].

As illustrated in Figs. 1(a) and 1(b), the β-V_2OPO_4 compound crystallizes in a bct structure with a space group $I4_1/amd$ (No. 141). The optimized lattice constants are $a = 5.465$ Å and $c = 12.544$ Å, which are in excellent agreement with the experimental values $a = 5.362$ Å and $c = 12.378$ Å [33]. The O atoms occupy two Wyckoff positions 4a (0.0,0.0,0.0) and 16h (0.000 00,0.237 62,0.432 99). The P and V atoms are located at the Wyckoff positions 4b (0.0,0.0,0.5) and 8c (0.250,0.000,0.875), respectively. The bct Brillouin zone (BZ) and (001) surface BZ are shown in Fig. 1(c), in which the high-symmetry points are marked.

We perform first-principles calculations using the Vienna *ab initio* simulation package (VASP) [37,38] based on density functional theory [39,40] (see more details in SM [36]). The random-phase approximation (RPA) is use to determine the magnetic configuration [41]. Our results confirm that the ground state of β-V_2OPO_4 is FM, which is about 57 meV lower than the AFM state per unit cell. The magnetic moment is $\sim 2.5\mu_B$ per V atom. The electronic band structure in the absence of SOC [see Fig. 2(a)] shows that the spins and orbitals are independent and two spin channels are decoupled around the Fermi level. These two spin channels present different electronic states, i.e., a ~3.68 eV band gap of the minority spin states and the semimetallic features of majority spin states, indicating the half-metallic properties of β-V_2OPO_4. The band crossings appear around the Γ point in the $k_z = 0$ plane, giving rise to a symmetry protected nodal-line loop. These two crossing bands belong to states that have opposite eigenvalues ± 1 of mirror reflection symmetry operation M_z, respectively, which protects the nodal ring in the k_x-k_y plane with $k_z = 0$ [10]. The spin-polarized nodal ring shows a tiny dispersion, and the maximal deviations are ~12 meV higher and ~36 meV lower from the Fermi level E_F in the Γ-X and Γ-Σ directions, respectively.

As shown in Fig. 2(b), the SOC has little influence on the band structure, and half-metallic ferromagnetism remains. The spontaneous magnetization direction is determined by studying the total energy of the system with magnetization along different high-symmetry axes. The [001] axis is found to be in the energetically most favorable magnetization direction. It is worth mentioning that all possible magnetic configurations are nearly degenerate, implying that the magnetism in β-V_2OPO_4 is "soft." The magnetic configurations can be switched easily by applying an external magnetic field. In the presence of SOC, magnetic symmetry is dependent on the direction of magnetization. We will respectively present the topological features of β-V_2OPO_4 for two typical magnetization directions of [001] and [110].

When the magnetization direction is along the [001] direction, the system symmetry is reduced to the point group C_{4h}, which is the subgroup of D_{4h}. For the C_{4h} group, the fourfold

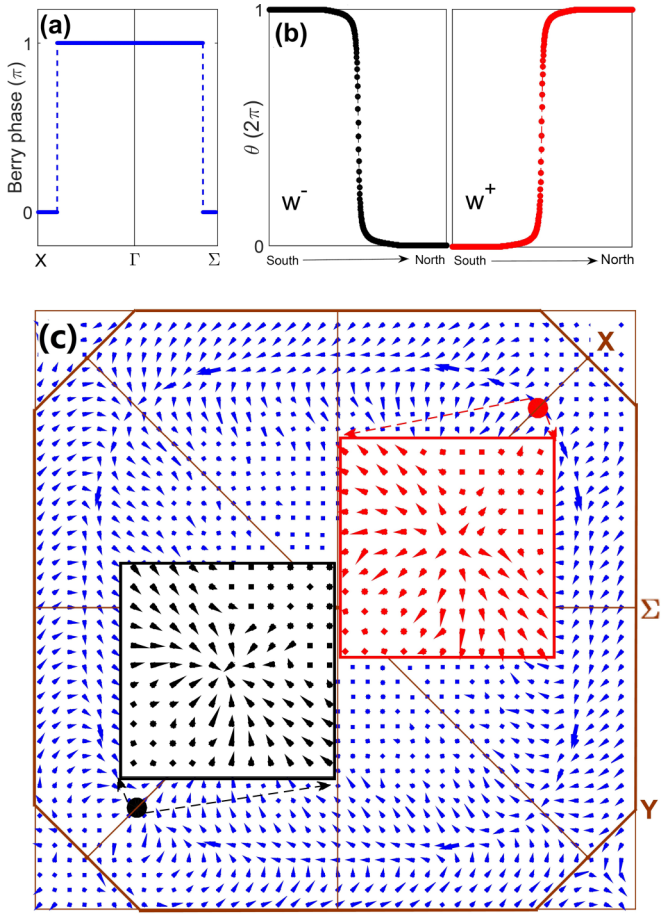

FIG. 3. (a) β-V_2OPO_4 with the magnetization direction along the [001] axis, and a variation of the Berry phase along the high-symmetry lines in a $k_z = 0$ plane. (b) With the magnetization direction along the [110] axis, the evolution of the average position of Wannier centers obtained by the Wilson-loop method applied on a sphere that encloses a Weyl point. The average Wannier center shifts downwards from south to north, indicating a negative chirality W^-. The average Wannier center shifts upwards from south to north, indicating a positive chirality W^+. (c) The distribution of Berry curvature for the $k_z = 0$ plane. The red and black regions denote the Weyl points with negative and positive chirality, respectively.

rotation C_4^z is tensored by inversion I, namely, $C_4^z \otimes I$. This magnetic group contains eight irreducible symmetry operators: inversion I, fourfold rotation C_4^z, the product of time reversal T and twofold rotations of C_2 symmetry axes [100], [010], [110], [1$\bar{1}$0], and the product (IC_2^z) of inversion I and rotation C_2^z. The group element IC_2^z is equivalent to the mirror reflection symmetry corresponding to the x-y plane, which can protect the existence of a gapless nodal ring in the $k_z = 0$ plane with respect to SOC [8,10,36] [see Fig. 2(b)]. The topological invariant of the nodal ring can be viewed as a variation of the quantized Berry phase with respect to the mirror plane [42], which is related to the change at the end of the one-dimensional system along a line across the ring in the $k_z = 0$ plane. As shown in Fig. 3(a), the Berry phase of β-V_2OPO_4 shows a jump across the ring, further confirming the topological features of the nodal ring perpendicular to the [001] magnetization direction.

Our calculations suggest that the magnetization along other directions is energetically nearly degenerate with the [001]. When the magnetization deviates from the [001] direction, mirror reflection symmetry is broken. Here, we take the case of [110] magnetization as an example since the symmetry analyses for other cases are essentially the same. The group elements of the corresponding magnetic space group C_{2h} remain: I, C_2^{110} and $TC_2^z, TC_2^{1\bar{1}0}$. The vanishing of mirror reflection symmetry makes the nodal line gapped. However, the antiunitary symmetry TC_2^z allows the existence of Weyl points in the $k_z = 0$ plane. A pair of Weyl points protected by C_2^{110} rotation is present on the $k_x = k_y$ axis (see SM [36]).

We also calculate the parities of inversion eigenvalues at all TRIM points. The product of the occupied bands running over all TRIM points is -1, confirming the presence of an odd number of pairs of Weyl points [28]. As shown in Fig. 2(b), the two crossing bands along Γ-X (or [110]) near the Fermi level belong to the irreducible representations Γ_3 and Γ_4 of C_2^{110}, respectively. The chirality of the Weyl point can be determined by the evolution of the average position of Wannier centers, and the Wilson-loop method applied on a sphere around a Weyl point is used [43,44] [see Fig. 3(b)]. The Weyl point with a Chern number $C = +1$ is located at (0.46 Å^{-1},0.46 Å^{-1},0) in momentum space, while the Weyl point with a Chern number $C = -1$ related by I symmetry is located at the same axis with a position of ($-$0.46 Å^{-1}, $-$ 0.46 Å^{-1},0) [see Fig. 1(c)]. The Weyl points only exist on the $k_x = k_y$ axis, which can be further verified by the Berry curvature. As shown in Fig. 3(c), the Weyl points with positive and negative chirality are regarded as the "source" and "sink" of the Berry curvature in momentum space.

As discussed above, our results indicate the existence of either FM topological NLSM or WSM phases in the β-V_2OPO_4 compound, depending on the magnetization direction. The other materials, such as Co_2S_2Tl and Fe_2S_2X (X = Al, Ga, In), exhibit similar band structures (see SM [36]). Their topological features are determined by magnetic symmetry and are not sensitive to chemical compositions. The specific NLSM features are protected by mirror reflection symmetry in the case of [001] magnetization, while the generic WSM features arise with a magnetization direction along another high-symmetry axis. The Weyl points would be protected by C_2^n rotational symmetry, where n represents a symmetry axis in the x-y plane. In comparison with isotropic magnetization in β-V_2OPO_4, we find that the magnetization directions of Co_2S_2Tl and Fe_2S_2X lying in the (001) (or x-y) plane are energetically most favorable [36]. Hence, the WSM features are dominated in these compounds with a FM ground state. For FM WSM, there only exists a pair of well-separated Weyl points, which is the minimum number of Weyl points in condensed matter systems. Considering that the energy of the Weyl points is very close to the Fermi level, e.g., ~12 meV with the [110] magnetization direction in FM β-V_2OPO_4, therefore, we suggest that our proposed compounds are excellent experimental candidates for the observation of the nontrivial properties in FM WSMs.

One hallmark of nontrivial semimetals is the existence of a topologically protected surface state, which arises from the inversion of band topology. Topological surface states connect

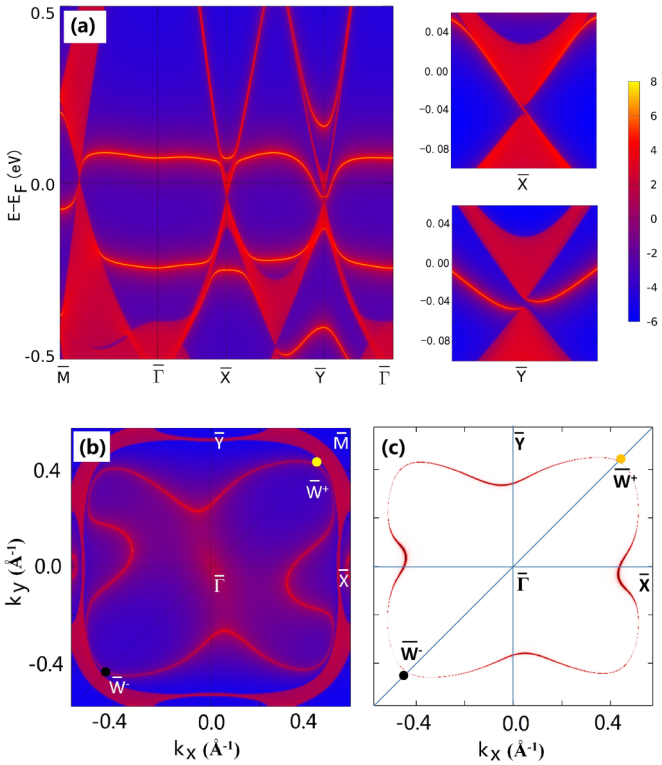

FIG. 4. Surface states and Fermi surfaces of β-V_2OPO_4 with magnetization along the [110] direction. (a) The energy bands projected on the (001) surface. In the left of (a), the upper and lower panels show magnified views of the regions near the $\bar{X}$ and $\bar{Y}$ points, respectively. (b) The corresponding Fermi surface for the (001) surface. The projected Fermi surface is calculated with a chemical potential at 60 meV above the Fermi level. (c) The spectral function with only a surface contribution of (b). The yellow and black dots in (b) and (c) denote the Weyl points with positive and negative chirality projected on the (001) surface, respectively.

the valence and conduction bands. The drumhead surface states of NLSMs will appear when the gap of the bulk band is closed, forming a nodal ring. Since the energy gap openings, except at the Weyl points of WSM, are very small, this makes only a tiny difference in the surface states between the NLSM and WSM phases. Here, we present the surface states and Fermi arcs in a [110] magnetic configuration. To obtain the surface states, we constructed a tight-binding (TB) Hamiltonian with a basis of maximally localized Wannier functions [45,46] in which the Green's function method [47] is employed as implemented in the WANNIERTOOLS code [48]. The calculated local density of states (LDOS) and Fermi surface projected on a (001) surface of β-V_2OPO_4 are shown in Figs. 4(a) and 4(b), respectively. The surface states are clearly observed in Fig. 4(a). On the (001) surface, the antiunitary magnetic symmetry TC_2 leads to different behaviors for the surface bands around $\bar{X}$ and $\bar{Y}$. Although some trivially residual bands would project on the (001) surface of this compound, the Fermi arc states denoted by the red line are quite clear, as shown in Figs. 4(b) and 4(c).

In conclusion, using first-principles calculations and topological constraints in a crystal with inversion symmetry, we theoretically identify a class of FM TSMs that can widely exist in centrosymmetric tetragonal structures, such as β-V_2OPO_4, Co_2S_2Tl, and Fe_2S_2X (X = Al, Ga, In). These materials can possess FM nontrivial properties of TSMs, either NLSMs or WSMs, that can be easily switched between each other by changing the magnetization directions. When the magnetization is along the [001] direction, these compounds present a gapless nodal ring at the k_x-k_y plane with $k_z = 0$ in momentum space, which is protected by mirror reflection symmetry. When the magnetization directions deviate from [001], the nodal ring will degenerate to a pair of Weyl points due to the vanishing of mirror reflection symmetry. These two Weyl points located at the k_x-k_y plane with $k_z = 0$ are well separated, protected by twofold rotational symmetry along the magnetization directions. All of the nontrivial band-crossing points are very close to the Fermi level, and the topology of the system is confirmed by the existence of nontrivial surface states. Our finding provides a realistic and promising platform for the investigation of FM TSMs in experiments, especially towards the realization of a quantum anomalous Hall effect in condensed matter systems.

This work is supported by the National Natural Science Foundation of China (Grants No. 11674148, No. 11304403, No. 11334003, and No. 11404159), the Natural Science Foundation of Guangdong Province for Distinguished Young Scholars (Grant No. 2017B030306008), and the Basic Research Program of Science, Technology and Innovation Commission of Shenzhen Municipality (Grant No. JCYJ20160531190054083).

Y.J.J., R.W., and Z.J.C. contributed equally to this work.

[1] X.-L. Qi, Y.-S. Wu, and S.-C. Zhang, Phys. Rev. B **74**, 085308 (2006).

[2] R. Yu, W. Zhang, H.-J. Zhang, S.-C. Zhang, X. Dai, and Z. Fang, Science **329**, 61 (2010).

[3] C.-Z. Chang, J. Zhang, X. Feng, J. Shen, Z. Zhang, M. Guo, K. Li, Y. Ou, P. Wei, L.-L. Wang *et al.*, Science **340**, 167 (2013).

[4] C. Fang, M. J. Gilbert, and B. A. Bernevig, Phys. Rev. Lett. **112**, 046801 (2014).

[5] C.-Z. Chang, W. Zhao, D. Y. Kim, H. Zhang, B. A. Assaf, D. Heiman, S.-C. Zhang, C. Liu, M. H. W. Chan, and J. S. Moodera, Nat. Mater. **14**, 473 (2015).

[6] G. Xu, H. Weng, Z. Wang, X. Dai, and Z. Fang, Phys. Rev. Lett. **107**, 186806 (2011).

[7] X. Wan, A. M. Turner, A. Vishwanath, and S. Y. Savrasov, Phys. Rev. B **83**, 205101 (2011).

[8] Z. Wang, M. G. Vergniory, S. Kushwaha, M. Hirschberger, E. V. Chulkov, A. Ernst, N. P. Ong, R. J. Cava, and B. A. Bernevig, Phys. Rev. Lett. **117**, 236401 (2016).

[9] A. A. Burkov, M. D. Hook, and L. Balents, Phys. Rev. B **84**, 235126 (2011).

[10] H. Weng, C. Fang, Z. Fang, B. A. Bernevig, and X. Dai, Phys. Rev. X **5**, 011029 (2015).

[11] S.-M. Huang, S.-Y. Xu, I. Belopolski, C.-C. Lee, G. Chang, B. Wang, N. Alidoust, G. Bian, M. Neupane, C. Zhang *et al.*, Nat. Commun. **6**, 7373 (2015).
[12] J. Ruan, S.-K. Jian, H. Yao, H. Zhang, S.-C. Zhang, and D. Xing, Nat. Commun. **7**, 11136 (2016).
[13] J. Ruan, S.-K. Jian, D. Zhang, H. Yao, H. Zhang, S.-C. Zhang, and D. Xing, Phys. Rev. Lett. **116**, 226801 (2016).
[14] G. Autès, D. Gresch, M. Troyer, A. A. Soluyanov, and O. V. Yazyev, Phys. Rev. Lett. **117**, 066402 (2016).
[15] Z. Wang, D. Gresch, A. A. Soluyanov, W. Xie, S. Kushwaha, X. Dai, M. Troyer, R. J. Cava, and B. A. Bernevig, Phys. Rev. Lett. **117**, 056805 (2016).
[16] Y. Xu, C. Yue, H. Weng, and X. Dai, Phys. Rev. X **7**, 011027 (2017).
[17] S.-Y. Xu, I. Belopolski, N. Alidoust, M. Neupane, G. Bian, C. Zhang, R. Sankar, G. Chang, Z. Yuan, C.-C. Lee *et al.*, Science **349**, 613 (2015).
[18] B. Q. Lv, H. M. Weng, B. B. Fu, X. P. Wang, H. Miao, J. Ma, P. Richard, X. C. Huang, L. X. Zhao, G. F. Chen *et al.*, Phys. Rev. X **5**, 031013 (2015).
[19] L. X. Yang, Z. K. Liu, Y. Sun, H. Peng, H. F. Yang, T. Zhang, B. Zhou, Y. Zhang, Y. F. Guo, M. Rahn *et al.*, Nat. Phys. **11**, 728 (2015).
[20] A. Tamai, Q. S. Wu, I. Cucchi, F. Y. Bruno, S. Riccò, T. K. Kim, M. Hoesch, C. Barreteau, E. Giannini, C. Besnard *et al.*, Phys. Rev. X **6**, 031021 (2016).
[21] M. Chinotti, A. Pal, W. J. Ren, C. Petrovic, and L. Degiorgi, Phys. Rev. B **94**, 245101 (2016).
[22] H. Yang, Y. Sun, Y. Zhang, W.-J. Shi, S. S. P. Parkin, and B. Yan, New J. Phys. **19**, 015008 (2017).
[23] J. Liu and D. Vanderbilt, Phys. Rev. B **90**, 155316 (2014).
[24] D. Bulmash, C.-X. Liu, and X.-L. Qi, Phys. Rev. B **89**, 081106 (2014).
[25] H. Chen, Q. Niu, and A. H. MacDonald, Phys. Rev. Lett. **112**, 017205 (2014).
[26] A. K. Nayak, J. E. Fischer, Y. Sun, B. Yan, J. Karel, A. C. Komarek, C. Shekhar, N. Kumar, W. Schnelle, J. Kübler *et al.*, Sci. Adv. **2**, e1501870 (2016).
[27] M. Hirschberger, S. Kushwaha, Z. Wang, Q. Gibson, S. Liang, C. A. Belvin, B. A. Bernevig, R. J. Cava, and N. P. Ong, Nat. Mater. **15**, 1161 (2016).
[28] T. L. Hughes, E. Prodan, and B. A. Bernevig, Phys. Rev. B **83**, 245132 (2011).
[29] A. M. Turner, Y. Zhang, R. S. K. Mong, and A. Vishwanath, Phys. Rev. B **85**, 165120 (2012).
[30] G. Bergerhoff, R. Hundt, R. Sievers, and I. D. Brown, J. Chem. Inf. Comput. Sci. **23**, 66 (1983).
[31] E. Benser, R. Glaum, T. Dross, and H. Hibst, Chem. Mater. **19**, 4341 (2007).
[32] M. Satyanarayana, R. S. Rao, V. Pralong, and U. V. Varadaraju, J. Electrochem. Soc. **164**, A6201 (2017).
[33] R. Glaum and R. Gruehn, Z. Kristallogr. **186**, 91 (1989).
[34] A. Newmark, G. Huan, M. Greenblatt, and M. Croft, Solid State Commun. **71**, 1025 (1989).
[35] S. Ronneteg, R. Berger, and G. André, J. Magn. Magn. Mater. **322**, 681 (2010).
[36] See Supplemental Material at http://link.aps.org/supplemental/10.1103/PhysRevB.96.201102 for the structures and topological features of Co_2S_2Tl and Fe_2S_2X (X = Al, Ga, In), and the symmetry analysis of the $\mathbf{k}\cdot\mathbf{p}$ Hamiltonian of the gapless nodal line and Weyl points protected by a magnetic space group. The details of the computational methods in first-principles calculations are given, which include Refs. [49–57].
[37] G. Kresse and J. Furthmüller, Phys. Rev. B **54**, 11169 (1996).
[38] G. Kresse and J. Furthmüller, Comput. Mater. Sci. **6**, 15 (1996).
[39] P. Hohenberg and W. Kohn, Phys. Rev. **136**, B864 (1964).
[40] W. Kohn and L. J. Sham, Phys. Rev. **140**, A1133 (1965).
[41] J. Harl, L. Schimka, and G. Kresse, Phys. Rev. B **81**, 115126 (2010).
[42] D. Vanderbilt and R. D. King-Smith, Phys. Rev. B **48**, 4442 (1993).
[43] R. Yu, X. L. Qi, A. Bernevig, Z. Fang, and X. Dai, Phys. Rev. B **84**, 075119 (2011).
[44] A. A. Soluyanov and D. Vanderbilt, Phys. Rev. B **83**, 035108 (2011).
[45] N. Marzari, A. A. Mostofi, J. R. Yates, I. Souza, and D. Vanderbilt, Rev. Mod. Phys. **84**, 1419 (2012).
[46] A. A. Mostofi, J. R. Yates, Y.-S. Lee, I. Souza, D. Vanderbilt, and N. Marzari, Comput. Phys. Commun. **178**, 685 (2008).
[47] M. P. L. Sancho, J. M. L. Sancho, and J. Rubio, J. Phys. F: Metal Phys. **14**, 1205 (1984).
[48] Q. Wu, S. Zhang, H.-F. Song, M. Troyer, and A. A. Soluyanov, arXiv:1703.07789.
[49] J. P. Perdew, K. Burke, and M. Ernzerhof, Phys. Rev. Lett. **77**, 3865 (1996).
[50] J. P. Perdew, K. Burke, and M. Ernzerhof, Phys. Rev. Lett. **78**, 1396 (1997).
[51] P. E. Blöchl, Phys. Rev. B **50**, 17953 (1994).
[52] G. Kresse and D. Joubert, Phys. Rev. B **59**, 1758 (1999).
[53] D. M. Ceperley and B. J. Alder, Phys. Rev. Lett. **45**, 566 (1980).
[54] H. J. Monkhorst and J. D. Pack, Phys. Rev. B **13**, 5188 (1976).
[55] A. I. Liechtenstein, V. I. Anisimov, and J. Zaanen, Phys. Rev. B **52**, R5467 (1995).
[56] M. A. Korotin, V. I. Anisimov, D. I. Khomskii, and G. A. Sawatzky, Phys. Rev. Lett. **80**, 4305 (1998).
[57] A. Liebsch, H. Ishida, and G. Bihlmayer, Phys. Rev. B **71**, 085109 (2005).